AIAA SciTech Forum
23-27 January 2023, National Harbor, MD & Online
AIAA SCITECH 2023 Forum

10.2514/6.2023-0209

# Aeroacoustic Optimization of VTOL Rotor Blades

Matthew A. Clarke*
*Massachusetts Institute of Technology, Cambridge, MA 02139*

Emilio Botero†
*Stanford University, Stanford, CA 94305, USA*

**Increased interest in urban air mobility has seen various efforts to design air transportation systems with smaller or even indistinguishable acoustic footprints. With many proposed concepts opting for open rotors, attention has accordingly been placed on the optimization of rotor blades. Unfortunately, many of the existing design tools are either sufficiently accurate but very slow or very fast but lack the required accuracy to facilitate design optimization. To address this emergent need, we present an inexpensive but suitably accurate approach for designing low-noise rotors for vertical and short takeoff and landing aircraft. This approach employs elliptic functions to parameterize the spanwise sectional properties of the rotor blade and takes advantage of recent advances in numerical computation, notably GPU acceleration and automatic differentiation. To demonstrate the versatility of this proposed approach, two design studies representing the most common scenarios of rotor blade operation are explored. The first is that of a lift-rotor, primarily used for hover, while the second is of a prop-rotor that typically operates throughout a wide range of flight conditions. The findings of this paper highlight that this new approach is capable of successfully generating optimal planforms in two orders of magnitude less time than the traditional parameterization approach, with guaranteed smoothness of the sectional properties.**

Downloaded by MIT LIBRARIES on January 21, 2023 | http://arc.aiaa.org | DOI: 10.2514/6.2023-0209

## Nomenclature

| | | |
|---|---|---|
| $A$ | = | blade cross-sectional area |
| $alt$ | = | altitude |
| BPF | = | blade passing frequency |
| $c$ | = | chord distribution |
| $c_l$ | = | sectional lift coefficient |
| $c_d$ | = | sectional drag coefficient |
| DL | = | disc loading |
| $M$ | = | Mach number |
| $n$ | = | radial station index |
| $num$ | = | number of [ ] |
| $p, q$ | = | elliptic function hyperperameters |
| $P_L$ | = | loading noise |
| $P_T$ | = | thickness noise |
| $R$ | = | tip radius |
| $r$ | = | non-dimensional radial distribution |
| $RPM$ | = | revolutions per minute |
| $\text{SPL}_A$ | = | A-weighted sound pressure level |
| $v$ | = | freestream velocity |
| $y$ | = | cosine-spaced radial distribution |
| $\beta$ | = | twist distribution |
| $\beta_0$ | = | blade root twist |
| $\beta_c$ | = | collective pitch |
| $\eta$ | = | aerodynamic efficiency |
| $\lambda$ | = | blade taper |
| $\sigma$ | = | solidity |
| $\zeta$ | = | normalized cosine radial location |
| $\theta$ | = | angular spanwise location |
| $\theta_e$ | = | noise evaluation angle |

**Subscripts**

| | | |
|---|---|---|
| $b$ | = | blade |
| $cr$ | = | cruise |
| $h$ | = | hub |
| $hov$ | = | hover |
| $OEI$ | = | one engine inoperative |
| $r$ | = | root |
| $t$ | = | tip |

**Superscripts**

| | | |
|---|---|---|
| $*$ | = | ideal condition |

*Postdoctoral Fellow, Department of Aeronautics and Astronautics
†Postdoctoral Scholar, Department of Aeronautics and Astronautics



Copyright © 2023 by Matthew Clarke. Published by the American Institute of Aeronautics and Astronautics, Inc., with permission.

Downloaded by MIT LIBRARIES on January 21, 2023 | http://arc.aiaa.org | DOI: 10.2514/6.2023-0209

# I. Introduction

Modern urban air mobility aircraft concepts possessing distributed electric propulsion architectures have long been regarded to offer several advantages over conventional helicopter or short takeoff and landing tube-and-wing concepts, particularly in the dimensions of maneuverability, redundancy, and compactness. These unique features make them ideal for operating in confined spaces such as cities, where space for arrival and departure is limited. That said, the impending introduction of large numbers of aircraft at low altitudes has not come across without justifiable push-back. Indeed, the livelihoods of entire communities will stand the risk of disruption from projected rises in noise levels [1]. Void of internal combustion machinery, the majority of noise emanating from many of these emerging eVTOL concepts arises from pressure disturbances generated by their rotating blades, along with the interactions between the helical wakes that these blades generate and the airframe. Designers are therefore faced with the task of minimizing radiated noise without sacrificing aerodynamic efficiency and structural integrity.

Numerous studies in the literature have explored rotor blade shape optimization using a variety of computational tools spanning all levels of modeling fidelity. Some adopt high-fidelity methods that are more accurate but computationally expensive like computational fluid dynamics and finite element analysis [2–5]. Others opt for medium-fidelity methods that simplify flow phenomena and/or blade geometry to garner faster approximations with an understanding that modeling accuracy will be impacted. Such medium-fidelity methods include blade element theory for estimating aerodynamic loads and beam models for estimating the incurred stresses [6–11]. Recent studies worth mentioning include Ning [12], who rearranged the classical blade element momentum theory (BEMT) formulation and leveraged Automatic Differentiation (AD) to obtain significant improvements in numerical stability and convergence of a gradient-based optimizer. This study however only examined the aerodynamic characteristics of the rotor blade. In another study by Ingraham and Gray [13], a BEMT formulation was coupled with a time-domain acoustic solver to optimize a propeller subject to aerodynamic and acoustic constraints. This study also did not cover any structural or material considerations of the blade. All three domains of aerodynamics, aeroacoustics and aerostructural analysis were however incorporated in separate studies by Gur and Rosen [14] and Stoll [15], who independently developed multi-disciplinary approaches for designing and analyzing rotors. Both studies utilized BEMT to capture aerodynamic loads, time-domain formulations of the Ffowcs-Williams/Hawkings equation to predict acoustic noise, and beam models to estimate normal and shear stress along the blade.

Common in all four studies was the adoption of the traditional approach to discretize the blade into spanwise sections. While this strategy has been shown to arrive at rotors with desired performance, sufficient parameter constraints along with a robust optimizer capable of computing analytical derivatives of the objective function to design variables are oftentimes required to guarantee the smoothness of blade features such as twist and chord. In the absence of AD, finite differencing is used, and gradient-based optimizers tend to get stuck in local minima caused by inaccurate gradients resulting in jagged blades as shown in Figure 1. To address this issue, a new approach in which the variation of features is controlled by continuous elliptic functions is proposed here. These functions are characterized by 4 parameters rather than the number of stations along the blade, which, for a typical blade discretization, can be upwards of 50 stations. Even without AD capability, the number of gradient evaluations required to make a finite difference step is significantly

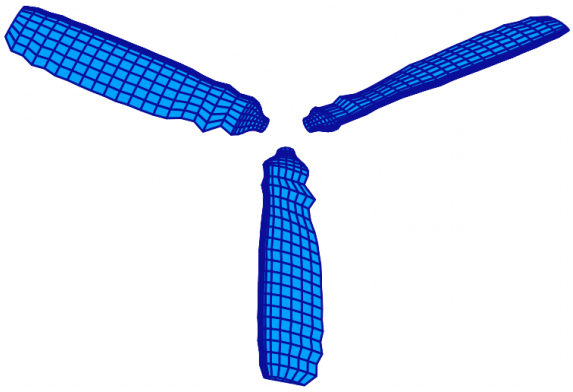

**Fig. 1 A lift-rotor design generated using the traditional approach and a gradient-based optimizer without AD capability. The jagged, non-smooth platform signified the optimizer terminating prematurely in a local minimum.**

reduced. With AD, finite difference operations are completely removed altogether, further accelerating the optimization routine.

Aerodynamic, aeroacoustic, and failure mode considerations of rotor blade design are examined in this paper. Since aerostructural analysis is omitted, it is assumed that the generated blades are strong enough to bear the forces and moments during nominal and emergency operations. It is also assumed that these blades are light, requiring minimum support at the hub. The remainder of this paper is broken down into five sections. Section II provides a qualitative assessment of how geometric properties and operating conditions impact a rotor's aeroacoustic and aerodynamic performance. This is followed by Section III which discusses in greater detail the general elliptic function used to parameterize sectional properties. Section IV summarizes the computational methods used in this study, then Section V expands upon the implementation of GPU acceleration and automatic differentiation in the SUAVE code framework used for managing the various optimization sub-routines. Optimization results are presented in Section VI. In this section, a comparison of the performance of traditional and newly proposed blade parameterization approaches is first presented. Design studies of a lift-rotor and prop-rotor are subsequently explored.

Downloaded by MIT LIBRARIES on January 21, 2023 | http://arc.aiaa.org | DOI: 10.2514/6.2023-0209

## II. Rotor Design Considerations

Whether the rotor is used primarily for high-speed forward flight (propeller), low-speed vertical flight (lift-rotor), or a combination of both (prop-rotor), there is a common design philosophy. This is depicted below in Figure 2. The various aspects of rotor blade design can be broken down into the three domains of material properties, operating loads, and certification criteria that the rotor has to meet. Each of them can comprise multiple disciplines which are quantified empirically, theoretically, or a combination thereof. These disciplines are then aggregated to arrive at a rotor with the desired characteristics.

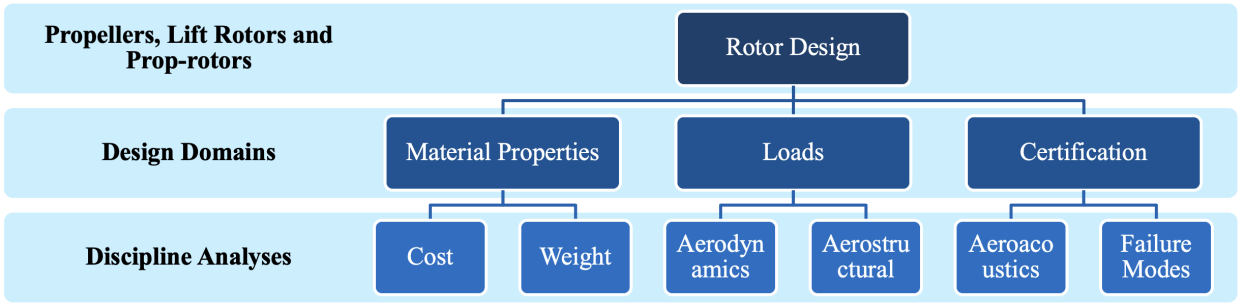


**Fig. 2 Rotor blade design considerations.**

An understanding of how a rotor's characteristic power spectral density could be influenced by an alteration of its geometric features or a modification of loads subjected to it by the working fluid is quintessential to elucidating trends unearthed during blade shape optimization. For both educational purposes as well as for reference later in the discussion of results in Section VI, a qualitative investigation of the aeroacoustic and aerodynamic responses to changes to an isolated rotor is provided below. We first make some remarks about a baseline rotor used as a reference point:

- The baseline rotor is operating its design point at peak aerodynamic efficiency at a specific advance ratio.
- The baseline rotor possesses a constant chord distribution and linear washout twist distribution from the rotor hub to the blade tip.

**Table 1 Rotor blade performance responses to design variable changes.**

| Acoustic Impact | Aerodynamic Impact |
|---|---|
| **I. Number of Blades** | |
| Increasing $num_b$ increases the BPF, diminishing the effect of A-weighting attenuation. | Increasing $num_b$ reduces $\eta$ due to wake interference and aerodynamic drag. |

| II. Solidity | |
|---|---|
| Lowering $\sigma$ reduces thickness noise as the volume displaced by each blade is reduced. A reduction in $\sigma$ means that either blade loading or $num_b$ must be increased to achieve the same $T$ at a given RPM | Keeping $R$ fixed and decreasing $\sigma$ however also improves $\eta$ of rotors. However, if $\sigma$ is too low, high angles of attack are needed to achieve the required lift, increasing drag. |
| **III. Tip Speed** | |
| Decreasing $M_t$ to a reduction in noise as the dominating $P_T$ in the far-field decays. | A change $M_t$ shifts the rotor's operating state away from its optimal point, worsening $\eta$. |
| **IV. Blade Loading** | |
| Lowering blade loading reduces $P_L$. However, to generate a given thrust, either the $num_b$ must increase. | For hovering rotors, the induced power loading is inversely proportional to $\sqrt{\text{DL}}$. In other words, as DL decreases, $\eta$ of the rotor increases. |
| **V. Blade Twist** | |
| Re-twisting the blade to move the majority of the load inboard redistributes acoustic energy from integer multiples of the BPF to lower harmonics which are penalized more by the A-weighting scale. | Shifting load distribution inboard increases $c_l$ near the hub. With airfoils no longer operating at their design $c_l$, a drop in performance will be experienced. |
| **VI. Blade Section Chord and Thickness** | |
| Increasing $t$ or $c$ increases $P_T$. Additionally, shifting the load toward the trailing edge causes phase lag which promotes phase cancellation[16]. | Increasing $A$ increases parasitic drag, resulting in a drop in $\eta$. Similar to **V**, this redistribution of aerodynamic loading will reduce $\eta$. |
| **VII. Rotor Radius** | |
| Reducing $R$ shifts the load distribution inward, causing more noise to be radiated at the lower harmonics. | Decreasing $R$ lowers $\eta$. |
| **VIII. Rotor Phasing** | |
| In-phase rotors amplify harmonic features of the acoustic spectrum increasing overall SPL. Out-of-phase rotors result in resonance cancellation and redistribute acoustic energy across the frequency spectrum, lowering SPL. | Provided rotors are sufficiently spaced apart, there is no significant impact on $\eta$. |
| **IX. Blade Spacing** | |
| Uneven blade spacing redistributes harmonic energy over the acoustic spectrum. | Generated tip vortices from the preceding blades reduce the efficiency of the ensuring blades. |
| **X. Blade Sweep** | |
| Sweeping the rotor blade de-phases the noise radiated from different portions of the blade, resulting in a redistribution of acoustic energy. | Drag on rotor blades can be reduced by sweeping the outboard sections of a blade which operate at higher Mach numbers[17]. Sweeping however can also induce out-of-plane hinge moments at the rotor hub. |

Downloaded by MIT LIBRARIES on January 21, 2023 | http://arc.aiaa.org | DOI: 10.2514/6.2023-0209

## III. Blade Design Methodology

As previously mentioned, the traditional approach to optimizing a rotor entails the discretization of its planform into spanwise quasi-two dimensional airfoils or blade sections, followed by the alteration of geometric properties to achieve the desired performance. Even with coarse discretization, say 50 radial stations, the number of design variables in the optimization problem can be quite large, with over 200 parameters, i.e. 50 values for the chord, twist, rake, and skew each. Moreover, should the designer additionally wish to modify the cross-sectional shape at each station using control points on the surface of airfoil sections, the total number of design variables can quickly surpass 10000 if each section is defined by 200 points. Using finite differences to obtain objective and constraint sensitivities to each of these variables during optimization can therefore be quite costly. With so many design variables, the odds that a gradient-based optimizer falls into local minima are relatively high, resulting in a final blade design with kinks or peculiar deformities

that for practical purposes would be difficult to manufacture even using the most sophisticated techniques of today.

A new approach for parameterizing features is proposed to overcome these challenges. Gaining inspiration from the work of Traub et al. [18], an elliptic shape function with a linear offset that yields a variety of permissible planforms shown in Figure 3 is used to generate possible distributions of any given characteristic. The general forms of this equation for the chord and twist distributions are provided below:

$$c_n = c_h(1 - \eta_n^p)^q + c_t\zeta_n, \tag{1a}$$

$$\beta_n = \beta_h(1 - \eta_n^p)^q + \beta_t\zeta_n + \beta_0 + \beta_c. \tag{1b}$$

The variables $[c_h, \beta_h]$ and $[c_t, \beta_t]$ are pivot points at the hub and tip sections for chord and twist respectively while $p$ and $q$ are hyperparameters of the elliptic function. In Equation 1b, $\beta_0$ is the root incidence angle that is uniformly added to the twist distribution. An additional parameter $\beta_c$ representing collective pitch control is also included to accommodate the design of variable-pitch rotors operating in more than one flight condition. The normalized spanwise location along the blade denoted $\zeta_n$, is defined below:

$$\zeta_n = \left|\frac{y_n}{r_t}\right|, \tag{2}$$

and corresponding of the spanwise station, $y_n$ is given by Equation 3a. The angular spanwise location, $\theta_n$, varies with the station index, $n$ along the blade where $n$ ranges from 0 to $N$-1. Here, $N$ is the total number of stations used to define the rotor blade.

$$y_n = r_t cos(\theta_n), \tag{3a}$$

$$\theta_n = \frac{n\pi}{2r}. \tag{3b}$$

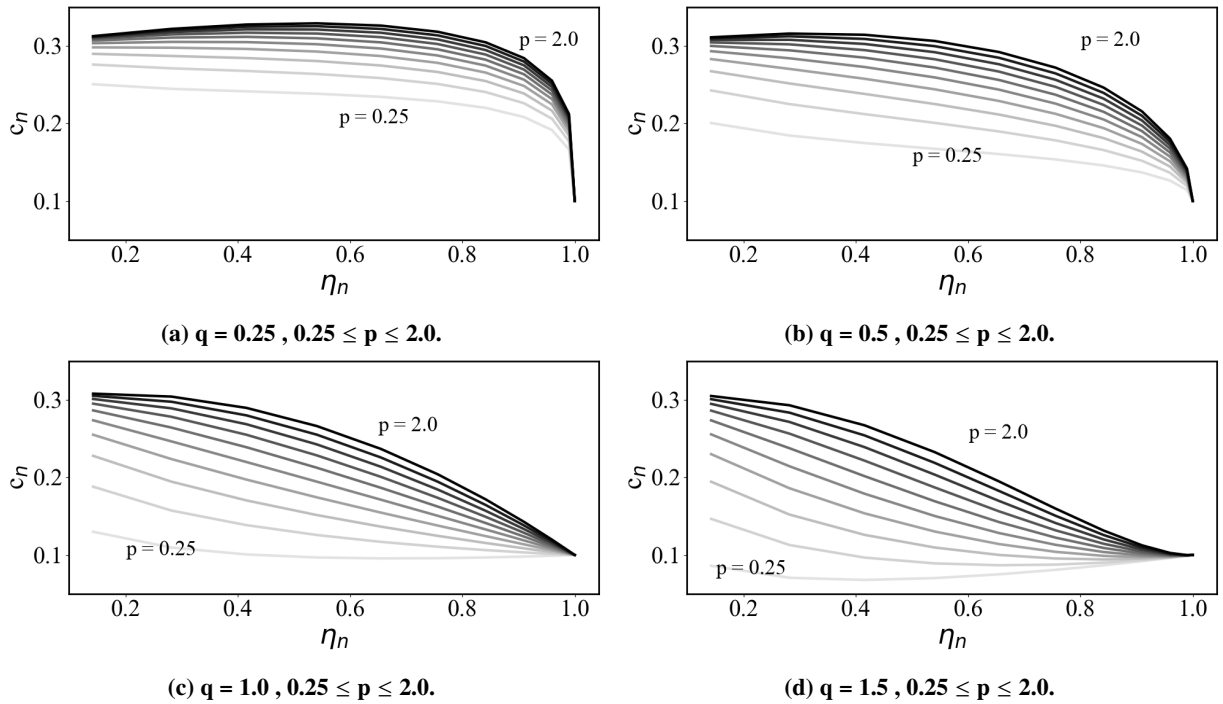


**(a) q = 0.25 , 0.25 ≤ p ≤ 2.0.** **(b) q = 0.5 , 0.25 ≤ p ≤ 2.0.**

**(c) q = 1.0 , 0.25 ≤ p ≤ 2.0.** **(d) q = 1.5 , 0.25 ≤ p ≤ 2.0.**

**Fig. 3 Blade feature parameterizing shape functions: $c_r$ = 0.3 and $c_t$ = 0.1.**

Downloaded by MIT LIBRARIES on January 21, 2023 | http://arc.aiaa.org | DOI: 10.2514/6.2023-0209

# IV. Computational Methods for Rotor Analysis

## A. Aerodynamics

Closely following the derivation in [19], a blade element model coupled with a vortex wake model (BET-VW) is used to compute aerodynamic loads generated by the rotor. Previously implemented and validated in SUAVE [20, 21], this model begins with a discretization of the blades into sections, each characterized by twist, chord, rake, and skew. Sectional forces are computed at the local Reynolds number and angle of attack by querying pre-built surrogate models of these aerodynamic force coefficients. Before querying the surrogates, an intermediary post-processing step of applying post-stall corrections based on the empirical correlations by Spera [22] is carried out. The sectional lift and drag forces are then decomposed into components parallel and perpendicular to the freestream to acquire distributions of thrust and torque along the blade. Prandtl tip and hub loss factors are applied to these distributions to account for three-dimensional effects, then finally the loads are integrated along the blade from hub to tip to obtain the total thrust and torque produced by the rotor.

## B. Aeroacoustics

Due to its computational efficiency coupled with satisfactory accuracy, a frequency-domain approach was preferred to a time-domain approach for predicting rotor noise in this study. For the harmonic noise contributions of the acoustic spectrum, expressions for thickness and loading noise by Hanson [23] are used. These expressions are capable of capturing the effects of blade thickness, non-axial inflow, and blade sweep, making them ideal for rotor optimization. A comprehensive derivation of these two expressions can be found in [24]. Despite referring to a collection of noise-generating phenomena – blade wake interaction (BWI), blade vortex interaction (BVI), turbulent and laminar boundary layers, blunt trailing edges, and tip vortices – only turbulent boundary layer-trailing edge (TBE-TE) of broadband noise is modeled in here. Even with the omission of these other sources, however, reasonable accuracy in uniform flow regimes where contributions of BWI and BVI are negligible is still achievable. TBE-TE noise is computed using Amiet's model [25] following the approach outlined by Li and Lee [26]. The process begins with using the outputs of a BEMT code to compute boundary layer properties using a panel method-boundary layer solver. These boundary layer properties are then passed as inputs into Lee's wall pressure spectrum model [27] which computes the characteristic noise spectrum.

# V. Numerical Considerations for Acceleration and Optimization with SUAVE

Since SUAVE's inception in 2013, it was intended for multifidelity analysis and optimization of advanced aircraft concepts [28–31]. To tackle these advanced aircraft concepts, no compromises were made in analysis capability towards the expense of optimization. Thus, for many years the primary means of gradient estimation was through finite-difference approximations. For many cases, especially those with fewer design variables, this was sufficient. However, building on the success of recent work introducing JAX [32] into SUAVE's Vortex Lattice Method [33] the next logical step was the rotor methods. JAX provides two primary benefits over ordinary Python and NumPy code as seen in SUAVE. First, it provides a just-in-time (JIT) compilation of code through XLA with support on both CPU and GPU. This enables both portability essential to testing and scaling, along with excellent speed. Second, JAX provides AD via its basis in Autograd. The results of both JIT and AD are multi-fold for SUAVE. First, repeated evaluations are significantly faster even after accounting for compilation costs. Second, gradient evaluations are negligibly slower than a primal function evaluation, especially when compared to finite-difference approximations. Prior SUAVE optimization problems spent the vast majority of their time calculating gradients. Finally, proper AD gradients are numerically exact to working precision.

The rotor methods provided a significant coding challenge to the developers. Although JAX provides support for Numpy code, it is not true "plug and play." JAX also provides limited support for SciPy code. Therefore significant refactoring of the code base was required while ensuring existing verification and validation efforts still hold. The underlying numerical solver of the BEMT wake solver initially relied on a simple newton method with analytical derivates which was later replaced by SciPy's fsolve and finite differencing as the methods became more complex. When viewed through the lens of an optimization algorithm, this means there is fundamentally an inner solver. This inner solve with fsolve itself requires gradient approximations and a numerical tolerance, thus providing extensive numerical noise to the optimization process. This numerical noise is the source of the jagged rotor seen in Figure 1. With fsolve not supported in JAX, we returned to a Damped Newton Method but this time with AD gradients within the inner solver.

Downloaded by MIT LIBRARIES on January 21, 2023 | http://arc.aiaa.org | DOI: 10.2514/6.2023-0209

This means two levels of gradients are passed through SUAVE, both an inner convergence layer and an outer high-level parameter layer. For the noise analyses, two specific functions required programming tricks. The Fresnel integrals and Bessel functions are not natively in NumPy, those are accessed through a "pure callback" to un-jitted code. Gradients are provided through hand-derived analytic expressions for those functions as a jacobian vector product.

The optimization process was provided through an updated SUAVE Nexus. This Nexus is fully JAX compatible and handles the objective gradients, constraint Jacobians, and interfacing with optimization packages. The user interfaces are left the same with extensive "under-the-hood" upgrades. In SUAVE, AD is done in forward mode due to the presence of for loops which require unrolling. Running the cases provided was done both via GPU and CPU acceleration using Pyoptsparse [34] and SNOPT [35]. Full optimization runs for lift rotors were performed on an Intel i9 CPU taking roughly 600 seconds while on an NVIDIA Tesla V100 times were approximately 90 seconds. These times also include the compilation time, which for this problem represents a significant fraction.

## VI. Discussion

Armed with a conceptual understanding of blade design, we shift our attention to specific examples where we seek to maximize performance while minimizing the radiated noise. Two design studies demonstrating the applicability of this newly proposed parameterization approach are explored. The first study was that of a lift-rotor used primarily for hover and vertical flight. The second design study was that of a prop-rotor used for wider ranges in flight conditions, for example, transitioning from low-speed vertical flight, through edgewise flight regimes, to finally high-speed cruises. To condense the disciplines of aerodynamics and aeroacoustics into one single objective, a weighted-exponential sum approach was selected due to the presumption of Pareto optimality. This approach combines goal programming and the weighted sum method whereby for each discipline, the distance between the solution point and a goal point in the criterion space is weighted [36]. The general form of this objective function is given below.

$$f(\mathbf{x}) = \sum_{i=1}^{m} w_i \left| \frac{f_i(\mathbf{x}) - y_i^{\text{goal}}}{y_i^{\text{goal}}} \right| \tag{4}$$

While portions of the Pareto optimal set can be obtained by continuously varying $p$, it is not guaranteed that the complete Pareto frontier is obtained [37]. Therefore, we vary the objective weights to generate possible blade designs on the Pareto frontier. Optimizer performance using the traditional parameterization (T.P.) approach as well as the newly proposed parameterization (N.P.) approach is depicted in Figure 4. To underscore the magnitude of the computational improvements to SUAVE, a further comparison between runs with and without using AD and GPU acceleration is provided. The light green and light blue lines depict runs on a CPU without AD, while the dark green and dark blue lines depict runs with AD enabled on a GPU. From this figure, it can be seen that a computational speed-up of upwards of two orders of magnitude was achieved along with improved numerical robustness. This finding is very powerful as it signals the possibility of embarking on more ambitious design exploration efforts like full vehicle optimization.

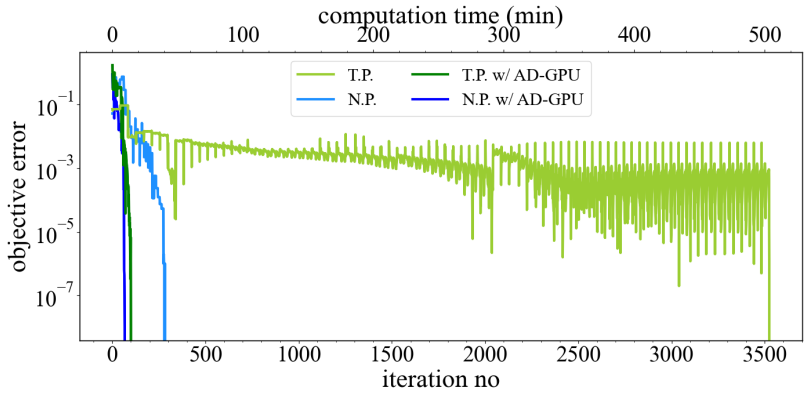


**Fig. 4 Rotor blade optimization convergence comparison of traditional and new parameterization approaches with and without AD and GPU acceleration.**

Downloaded by MIT LIBRARIES on January 21, 2023 | http://arc.aiaa.org | DOI: 10.2514/6.2023-0209

### A. Lift-Rotor Blade Design

We first begin with the examination of lift-rotors, used primarily for vertical flight. Shown in Table 2 are high-level physical attributes as well as the operating conditions of the rotor. The design load of 2943 N represents the amount of thrust each rotor of the 8-rotor stopped-rotor eVTOL aircraft shown in Figure 5 is expected to generate in hover. Table 3 lists each design variable in the optimization including the airfoil used for the blade's cross-section along the entire span of the blade. Since no aerostructural analysis is considered here, a minimum taper constraint was specified to ensure that the blade's structural integrity was not compromised – thin blade tips can break under extreme loading. Additionally, an upper bound on tip Mach number of 0.7 was instituted to ensure that the blades operate in the subsonic regime. This upper bound however was relaxed to 0.85 for the OEI condition, where each rotor is expected to produce 3924 N of thrust. This particular value was determined by computing the total thrust and then dividing by 6 to simulate a scenario where one rotor is inoperative and the pilot completely throttles down a diagonally offset rotor to maintain control authority. In the optimization problem defined in Table 3, $\alpha$ is an aeroacoustic objective weight and the goal points representing peak propulsive efficiency and low (ambient background) noise are 1 and 30 dBA respectively.

The trade-off between the consumed power and rotor noise is best understood using Figure 6a where a Pareto frontier does indeed capture their inverse relationship – aerodynamically efficient blades generate higher SPLs. This distribution of designs within the figure agrees with design intuition whereby as $\alpha$ decreases from 1 to 0, that is, moves from biasing aerodynamic efficiency to biasing aeroacoustic performance, power consumption increases. Figure 6b on the right depicting a similar Pareto suggests that reducing blade tip speed is an effective way of reducing radiated noise from the rotor. An explanation for how this is brought about is conveyed by blade RPM in Figure 7. Lowering the tip speed would generate harmonic tones at lower frequencies which would experience a more significant attenuation by the A-weighting scale.

Figures 6c and 6d provide further insight into the topology of low-noise lift-rotors. At the low inflow speeds experienced during hover, the optimizer seeks to increase the sectional chord near the hub to generate the same sectional lift coefficient produced at the blade tip. Had the taper constraint not been enforced, the planform for the most aerodynamically efficient blade would approach similar twist and chord distributions to a blade designed using the method put forth by Adkins and Liebeck [11]. Originally developed for designing propellers, their approach utilizes a closed-form solution that achieves a constant sectional lift coefficient along the blade. It however lacks taper constraints resulting in the generation of triangular-shaped blades at low inflow speeds.

Figures 6e and 6f give us a more apparent explanation of design variable sensitivity. It can be gathered from these figures that low noise-rotor designs tend to have higher loading near the blade tips compared to more aerodynamically efficient loads. At first, it may appear confusing why increasing solidity and twist distributions in addition to increasing outboard loading would lead to a reduction in noise. After all, each of these circumstances contradicts the qualitative discussion held in Section II. However, one must recall that these characteristics manifest in conjunction with a reduction in RPM. Such a finding suggests the effect of RPM outweighs other geometric and loading characteristics.

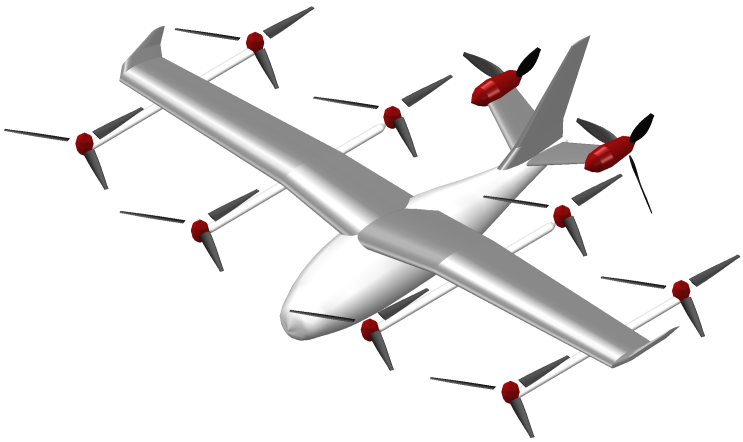

**Fig. 5 Six-passenger stopped-rotor eVTOL aircraft with 8 lift-rotors for vertical lift and 2 aft propellers for forward thrust.**



Downloaded by MIT LIBRARIES on January 21, 2023 | http://arc.aiaa.org | DOI: 10.2514/6.2023-0209

**Table 2 Lift-rotor design parameters.**

| Parameter | Value | Notes |
|---|---|---|
| $R_t$ | 1.350 m | tip radius |
| $R_h$ | 0.202 m | hub cut-out radius ($0.15R_t$) |
| $num_b$ | 3 | three-bladed rotor |
| airfoil | NACA 4412 | constant airfoil sections along the blade |
| $T_{hov}$ | 2943 N | all 8 rotors are operational |
| $alt_{hov}$ | 20 ft | hover altitude |
| $\theta_{e_{hov}}$ | 135° | 45° below the rotor plane |
| $v_{hov}$ | 0 | hover condition |
| $T_{OEI}$ | 3924 N | 6 operating rotors (OEI and throttling down diagonal rotor) |

**Table 3 Lift-rotor optimization problem setup.**

| | Parameter | Mathematical Expression | Optimization Notes |
|---|---|---|---|
| **Objective** | $f(\mathbf{x})$ | $f(\mathbf{x}) = \alpha\left(\left\lvert\frac{(FM-FM^*)}{FM^*}\right\rvert\right) + (1-\alpha)\left(\left\lvert\frac{(SPL-SPL^*)}{SPL^*}\right\rvert\right)$ | multi-objective function |

| | Parameter | Bounds [lower, upper] | Optimization Notes |
|---|---|---|---|
| **Design Variables** | $M_{t_{hov}}$ | $[0.3, 0.7]$ | subsonic limit |
| | $M_{t_{OEI}}$ | $[0.3, 0.85]$ | transonic limit |
| | $c_h$ | $[0.05R, 0.2R]$ | blade chord at rotor hub |
| | $c_t$ | $[0.02R, 0.1R]$ | tip chord |
| | $p_c$ | $[0.25, 2.0]$ | elliptic function hyperparameter |
| | $q_c$ | $[0.25, 1.5]$ | elliptic function hyperparameter |
| | $\beta_h$ | $[0, 45°]$ | blade twist at rotor hub |
| | $\beta_t$ | $[-5°, 45°]$ | tip twist |
| | $p_\beta$ | $[0.25, 1]$ | elliptic function hyperparameter |
| | $q_\beta$ | $[0.25, 0.5]$ | elliptic function hyperparameter |
| | $\beta_0$ | $[-30°, 30°]$ | hub incidence angle |
| | $\beta_{c_{hov}}$ | $[-30°, 30°]$ | hover collective pitch |
| | $\beta_{c_{OEI}}$ | $[-30°, 30°]$ | OEI collective pitch |
| | **Parameter** | **Conditions** | **Optimization Notes** |
| **Constraints** | $T_{hov}$ | $= T^*_{hov}$ | nominal operating condition |
| | $T_{OEI}$ | $\geq T^*_{OEI}$ | failure mode hover condition |
| | $c_{l_{hov}}$ | $\leq 0.8$ | hover $c_l$ limit |
| | $\lambda$ | $\geq 0.3$ | blade taper constraint |
| | $c_p/c_q$ | $\geq 0.5$ | elliptic function constraint |
| | $\beta_p/\beta_q$ | $\geq 0.5$ | elliptic function constraint |

Downloaded by MIT LIBRARIES on January 21, 2023 | http://arc.aiaa.org | DOI: 10.2514/6.2023-0209

Downloaded by MIT LIBRARIES on January 21, 2023 | http://arc.aiaa.org | DOI: 10.2514/6.2023-0209

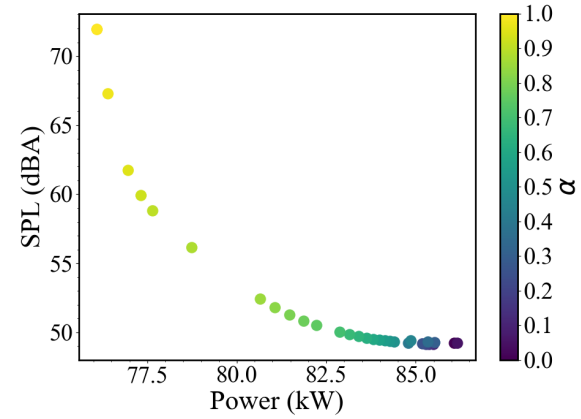


(a) Aeroacoustic objective distribution of rotor designs.

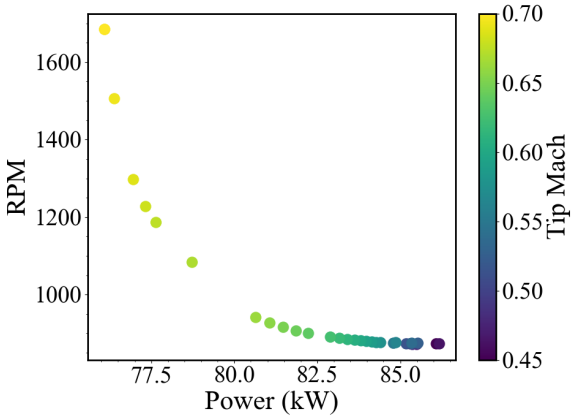


(b) RPM distribution of rotor designs.

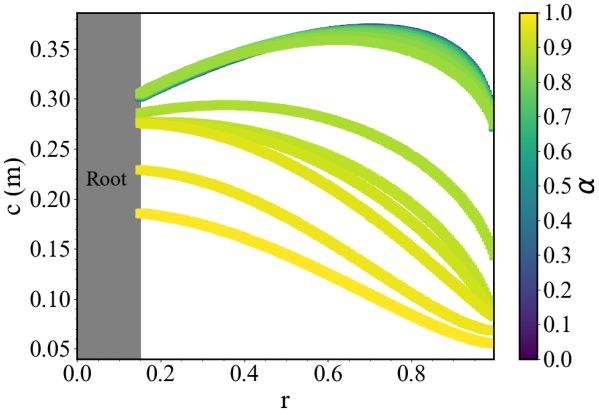


(c) Chord distribution.

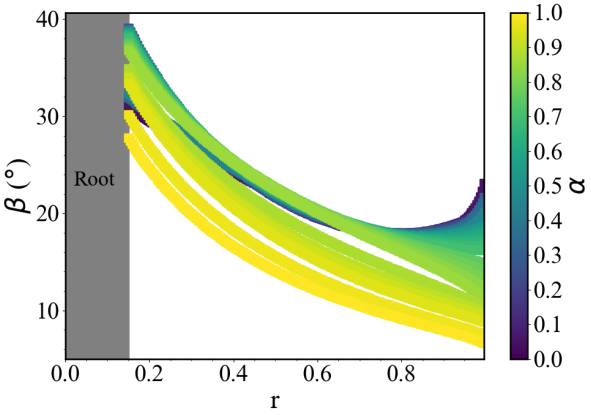


(d) Twist distribution.

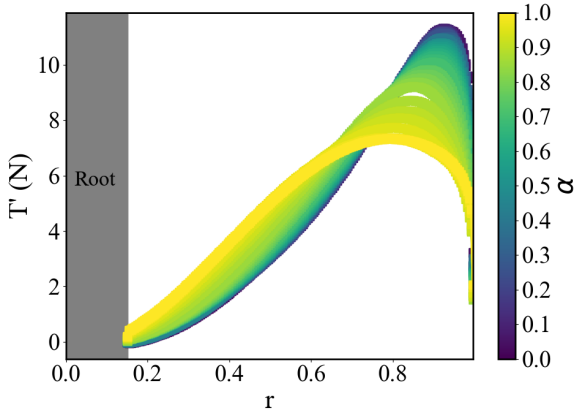


(e) Differential thrust distribution.

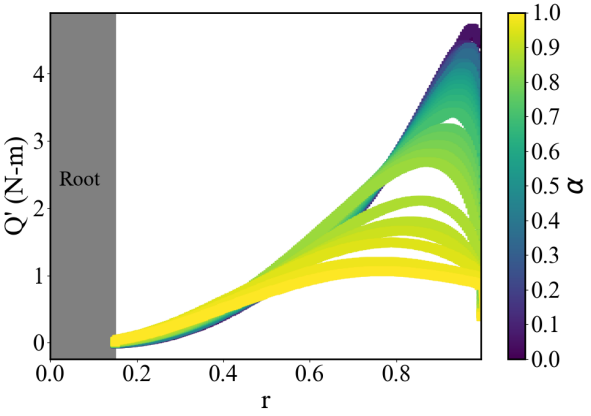


(f) Differential torque distribution.

**Fig. 6 Comparison of lift-rotor blade designs with $0 \geq \alpha \leq 1$.**

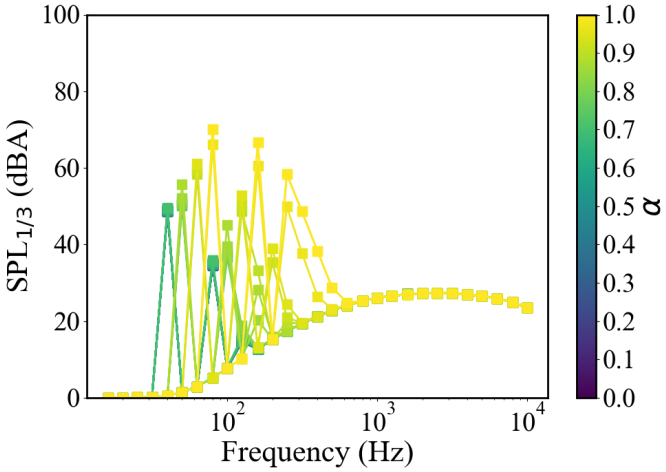


**Fig. 7 ⅓ Octave band spectra of optimized lift-rotor designs.**

Downloaded by MIT LIBRARIES on January 21, 2023 | http://arc.aiaa.org | DOI: 10.2514/6.2023-0209

### B. Prop-Rotor Blade Design Study

The design of prop-rotors is a little bit more involved as these types of rotors are not only characterized by heavy blade loading at lower airspeeds bit reduced blade loading at higher airspeeds. To achieve better efficiencies through the various flight regimes, they often operate with collective or variable pitch control. At lower airspeeds, blade pitch is reduced to ensure that the component of the freestream parallel to the rotor plane is higher than the perpendicular component of the inflow. At higher airspeeds, blade pitch is increased to prevent the blades from stalling. Despite there existing virtually an infinite set of design conditions and loads for which blade shapes can be generated, there are a few strategies that are commonly adopted for arriving at a suitable prop-rotor design. The first strategy is to design the rotor for a single design condition and use collective pitch to maximize the rotor blade's performance. An issue with this approach however is that this single-point design must be chosen judiciously. The second strategy is to select two design conditions, say the extremities of hover and cruise, and use a multi-objective optimization strategy to arrive at a single optimal design. These first two strategies do not require the designer to simulate the entire mission profile a priori. The third strategy however does and involves using an entire mission analysis to construct an objective function. For instance, the designer first determines what flight segments dominate with respect to power consumption and noise, then formulates an objective function accordingly.

In this paper, the second strategy is adopted whereby design loads were taken from the flight conditions of the tilt-rotor eVTOL aircraft shown in Figure 8. The nominal design loads for hover and cruise were 3862.5 N and 666.6 N respectively. Computed in a similar manner to the lift-rotor case, the thrust at the OEI condition was determined to be 5793.8 N. Table 5 provides the other design conditions used to set up the optimization problem given in Table 5. This table also details all of the design variables and constraints for the objective function. The tip Mach number was allowed to vary between 0.3 and 0.7, while the blade collective pitch was allowed to vary between ± 30° for the cruise and OEI conditions. In addition to the aeroacoustic objective weight previously discussed, two additional weights, $\beta$ and $\gamma$ were introduced in the objective function. As a note to the reader, $\beta$ here is not to be confused with the twist distribution. These weights enabled the designer to prioritize hover performance over the cruise performance or to prioritize the hover noise over the cruising noise in the second instance via $\beta$ and $\gamma$, respectively. This optimization problem can be simplified with the assertion that we are only concerned with vehicle noise when the aircraft is near the ground, i.e. hover, such that $\gamma$ can be set to 1. This reduces the number of objective weights to two, $\alpha$ and $\beta$. Two design studies are explored below. The first study keeps $\beta$ constant while examining different values of $\alpha$. The second study holds $\alpha$ constant while examining a change in $\beta$.

Downloaded by MIT LIBRARIES on January 21, 2023 | http://arc.aiaa.org | DOI: 10.2514/6.2023-0209

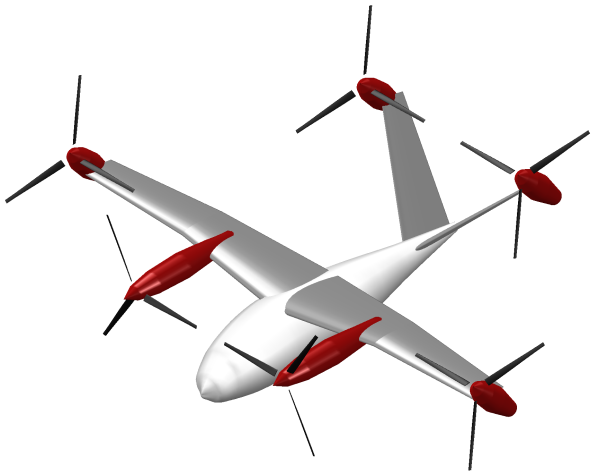

**Fig. 8 Six-passenger tilt-rotor eVTOL aircraft with 6 prop-rotors.**

**Table 4 Prop-rotor design parameters.**

| Parameter | Value | Notes |
|---|---|---|
| $R_t$ | 1.5 m | tip radius |
| $R_h$ | 0.22 m | hub cut-out radius ($0.15R_t$) |
| $num_b$ | 3 | three-bladed rotor |
| airfoil | NACA 4412 | constant airfoil sections along the blade |
| $T_{hov}$ | 3862.5 N | all 6 rotors are operational |
| $T_{cr}$ | 666.6 N | all 6 rotors are operational |
| $alt_{hov}$ | 20 ft | hover altitude |
| $alt_{cr}$ | 3000 ft | cruise altitude |
| $\theta_{e_{hov}}$ | 135° | 45° below the rotor plane |
| $v_{hov}$ | 0 | hover condition |
| $v_{cr}$ | 175 mph | cruise airspeed |
| $T_{OEI}$ | 5793.8 N | 4 operating rotors (OEI and throttling down diagonal rotor) |

**Table 5 Prop-rotor optimization problem setup.**

| | Parameter | Mathematical Expression | Optimization Notes |
|---|---|---|---|
| **Objective** | $f(\mathbf{x})$ | $f(\mathbf{x}) = \alpha f_{aero.} + (1-\alpha) f_{acous.}$<br>where,<br>$f_{aero.} = \beta \left( \left\| \frac{(FM_{hov} - FM^*)}{FM^*} \right\| \right) +$<br>$(1-\beta) \left( \left\| \frac{(\eta_{cr} - \eta^*)}{\eta^*} \right\| \right)$<br>$f_{acous.} = \gamma \left( \left\| \frac{(SPL_{hov} - SPL^*)}{SPL^*} \right\| \right) +$<br>$(1-\gamma) \left( \left\| \frac{(SPL_{cr} - SPL^*)}{SPL^*} \right\| \right)$ | multi-objective function |

| | Parameter | Bounds [lower, upper] | Optimization Notes |
|---|---|---|---|
| **Design Variables** | $M_{t_{hov}}$ | $[0.3, 0.7]$ | subsonic limit |
| | $M_{t_{OEI}}$ | $[0.3, 0.85]$ | transonic limit |
| | $M_{t_{cr}}$ | $[0.3, 0.7]$ | subsonic limit |
| | $c_h$ | $[0.05R, 0.2R]$ | blade chord at rotor hub |
| | $c_t$ | $[0.02R, 0.1R]$ | tip chord |
| | $p_c$ | $[0.25, 2.0]$ | elliptic function hyperparameter |
| | $q_c$ | $[0.25, 1.5]$ | elliptic function hyperparameter |
| | $\beta_h$ | $[0, 45°]$ | blade twist at rotor hub |
| | $\beta_t$ | $[-5°, 45°]$ | tip twist |
| | $p_\beta$ | $[0.25, 1]$ | elliptic function hyperparameter |
| | $q_\beta$ | $[0.25, 0.5]$ | elliptic function hyperparameter |
| | $\beta_0$ | $[-30°, 30°]$ | hub incidence angle |
| | $\beta_{c_{OEI}}$ | $[-30°, 30°]$ | OEI collective pitch |
| | $\beta_{c_{cr}}$ | $[-30°, 30°]$ | cruise collective pitch |
| | **Parameter** | **Conditions** | **Optimization Notes** |
| **Constraints** | $T_{hov}$ | $= T^*_{hov}$ | nominal hover condition |
| | $T_{OEI}$ | $= T^*_{OEI}$ | failure mode hover condition |
| | $T_{cr}$ | $= T^*_{cr}$ | nominal cruise condition |
| | $c_{l_{hov}}$ | $\leq 0.8$ | hover $c_l$ limit |
| | $c_{l_{cr}}$ | $\leq 0.8$ | cruise $c_l$ limit |
| | $\lambda$ | $\geq 0.3$ | blade taper constraint |
| | $c_p/c_q$ | $\geq 0.5$ | elliptic function constraint |
| | $\beta_p/\beta_q$ | $\geq 0.5$ | elliptic function constraint |

Downloaded by MIT LIBRARIES on January 21, 2023 | http://arc.aiaa.org | DOI: 10.2514/6.2023-0209

*1. Prop-Rotor Design Example: A Comparison of Aeroacoustic Objective Weighting*

Two prop-rotor designs with $\alpha = 0.9$ and $\alpha = 0.2$ are assessed here. The value of $\beta$ was held fixed at 0.5, implying that the cruise efficiency and hover figure of merit were weighted equally by the optimizer. Table 6 provides a summary of the optimization results. We see that prop-rotor A does indeed have higher efficiency than blade B, requiring 6.3% less power in hover and 17.4% less power in cruise. This, however, comes at the expense of noise. In the hover condition, this blade is about 16.92 dBA louder than prop-rotor B. Examining the cruise flight conditions more closely, it was observed that both the collective pitch and tip Mach number constraints are active - the collective pitches are driven to the upper bound of 30° while the blade tip Mach numbers are driven to the lower bound of 0.3.

From the 3D renderings of the rotor in Figures 9a and 9b along with the planforms in Figure 10a and 10b, it can be concluded that low-noise prop-rotor designs are indeed distinguished by higher solidity. Figures 11a and 11b also highlight another unique characteristic of prop-rotors. In cruise conditions, these rotors tend to carry the majority of the loading in the outboard sections of the blades while allowing the inboard sections near the hub to stall. Even with the aid of collective pitch, this poor aerodynamic efficiency on the inboard sections comes from the trade-off that these blades make to ensure that the blades are able to generate sufficient thrust at low airspeeds during hover and vertical flight.

**Table 6 Performance of two prop-rotor blade designs at a constant $\beta$ value of 0.5 and $\alpha$ values of 0.9 and 0.2.**

| | Parameter | Prop-rotor A | Prop-rotor B |
|---|---|---|---|
| Optimization Weights | $\alpha$ | 0.9 | 0.2 |
| | $\beta$ | 0.5 | 0.5 |
| | $\gamma$ | 1.0 | 1.0 |
| Hover Flight Condition | Collective Pitch (°) | 0.0 | 0.0 |
| | SPL (dBA) | 66.62 | 49.7 |
| | Power (kW) | 107.7 | 114.9 |
| | Tip Mach | 0.58 | 0.37 |
| OEI Flight Condition | Collective Pitch (°) | 20.88 | 6.82 |
| | Power (kW) | 941.5 | 798.1 |
| | Tip Mach | 0.68 | 0.58 |
| Cruise Flight Condition | Collective Pitch (°) | 30.0 | 27.4 |
| | Power (kW) | 65.9 | 79.6 |
| | Tip Mach | 0.36 | 0.30 |

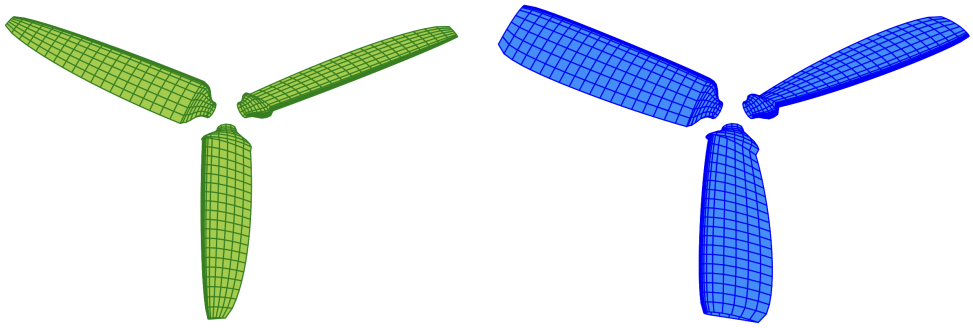

**(a) Prop-rotor A with $\alpha$ = 0.9.** **(b) Prop-rotor B with $\alpha$ = 0.2.**

**Fig. 9 Optimized prop-rotor designs with a constant $\beta$ of 0.5.**

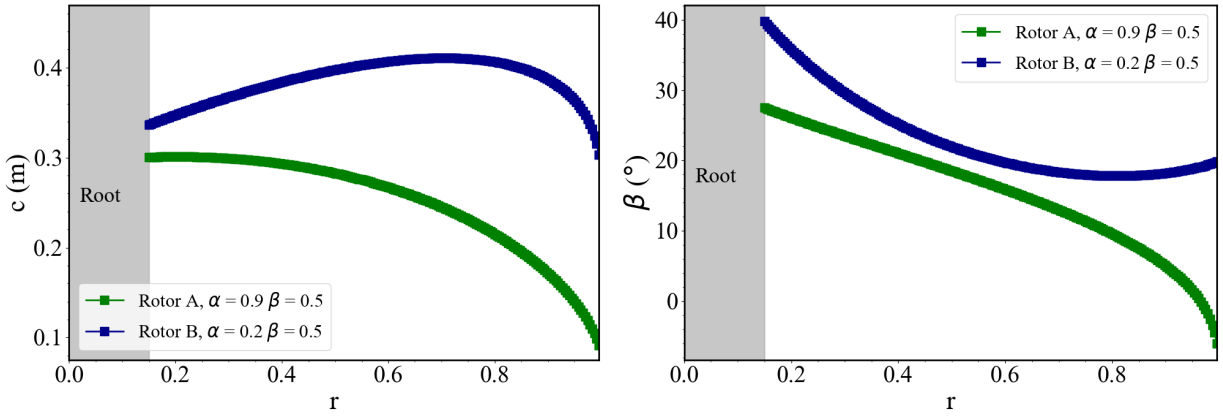


**(a) Chord distribution.** **(b) Twist distribution.**

Downloaded by MIT LIBRARIES on January 21, 2023 | http://arc.aiaa.org | DOI: 10.2514/6.2023-0209

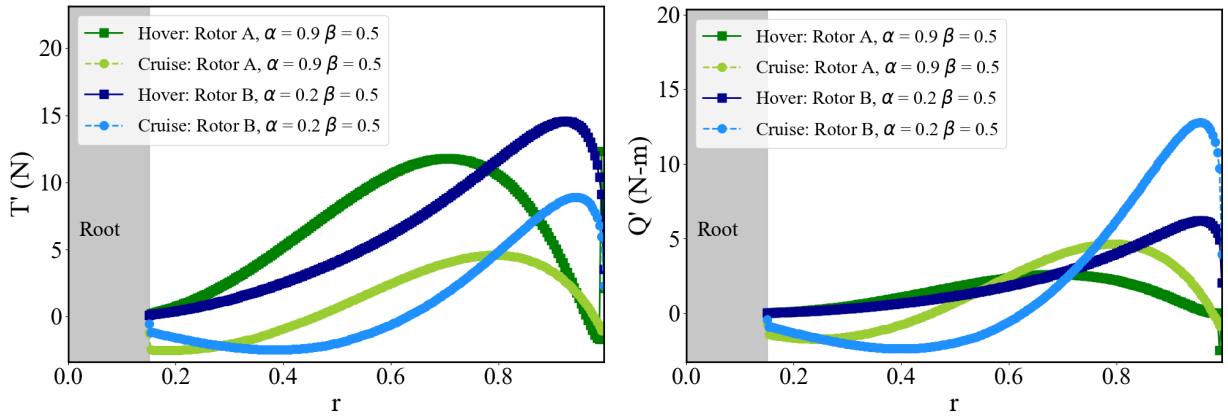


**(a) Thrust distribution.** **(b) Torque distribution.**

**Fig. 11 Prop-rotor planforms and performance at a constant $\beta$ of 0.5.**

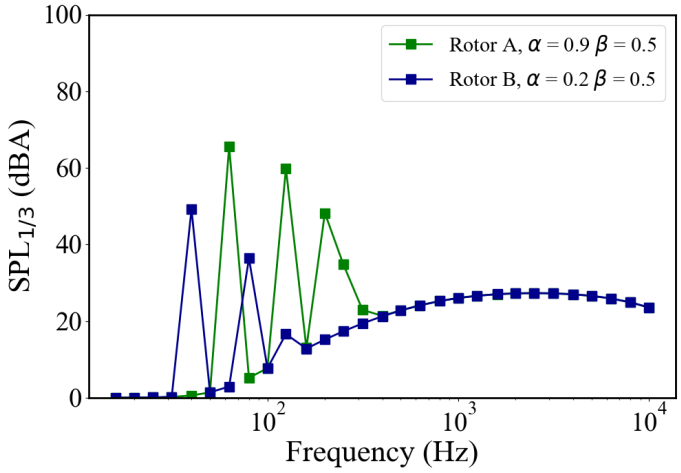


**Fig. 12 ⅓ Octave band spectra of prop-rotors at a constant $\beta$ of 0.5.**

*2. Prop-Rotor Design Example: A Comparison of Flight Condition Objective Weighting*

In this second study, the aeroacoustic objective weight was held fixed at $\alpha$ = 0.8 while the flight condition objective weight was varied. Referring back to the optimization problem, the higher the value of $\beta$, the greater the performance of the rotor in hover is biased. In other words, prop-rotor A prioritizes the rotor's efficiency in cruise while prop-rotor B prioritizes the rotor's figure of merit in hover. The results in Table 7 however only partially support this conjecture, as prop-rotor A not only outperforms prop-rotor B in cruise but also by a small margin in hove as well. A plausible hypothesis for this observation is that since the power consumption of the rotor is a less sensitive parameter to changes in geometric attributes and RPM than rotor noise, prop-rotor A is able to achieve the design thrust at a lower power value even though the noise of this rotor is 4.5 dbA higher than prop-rotor B. This contrast in relative sensitivities can be in fact seen in Figure 6a in Section VI.A where the range of noise is approximately 23 dbA but the range of power consumed is around 11.5 kW. Nevertheless, the almost identical blade topologies portrayed in Figure 13a and 13b in addition to the slight differences in noise and propulsive efficiency suggest that this particular optimization weight is not as significant as the aeroacoustic weight in the optimization process.



Downloaded by MIT LIBRARIES on January 21, 2023 | http://arc.aiaa.org | DOI: 10.2514/6.2023-0209

**Table 7 Performance of two prop-rotor blade designs at a constant $\alpha$ value of 0.8 and $\beta$ values of 0.1 and 0.9.**

| | Parameter | Prop-rotor A | Prop-rotor B |
|---|---|---|---|
| Optimization Weights | $\alpha$ | 0.8 | 0.8 |
| | $\beta$ | 0.1 | 0.9 |
| | $\gamma$ | 1.0 | 1.0 |
| Hover Flight Condition | Collective Pitch (°) | 0.0 | 0.0 |
| | SPL (dBA) | 57.2 | 52.7 |
| | Power (kW) | 107.4 | 109.3 |
| | Tip Mach | 0.42 | 0.39 |
| OEI Flight Condition | Collective Pitch (°) | 12.80 | 1.55 |
| | Power (kW) | 269.7 | 252.1 |
| | Tip Mach | 0.66 | 0.49 |
| Cruise Flight Condition | Collective Pitch (°) | 30.0 | 28.8 |
| | Power (kW) | 64.5 | 69.5 |
| | Tip Mach | 0.30 | 0.30 |

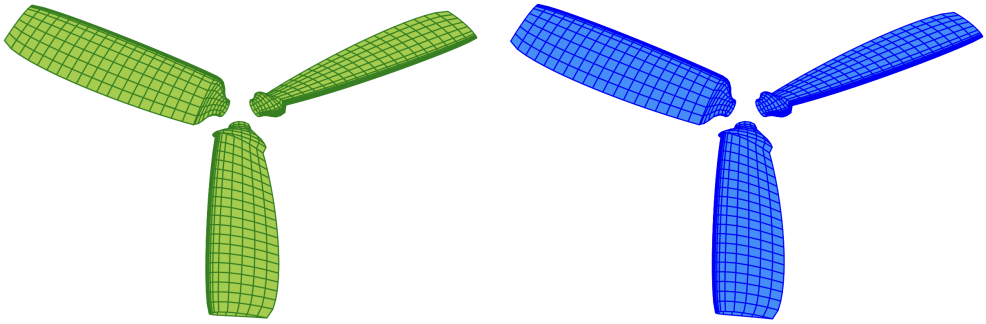

**(a) Prop-rotor A.** **(b) Prop-rotor B.**

**Fig. 13 Prop-rotor blade designs with a constant $\alpha$ of 0.8.**

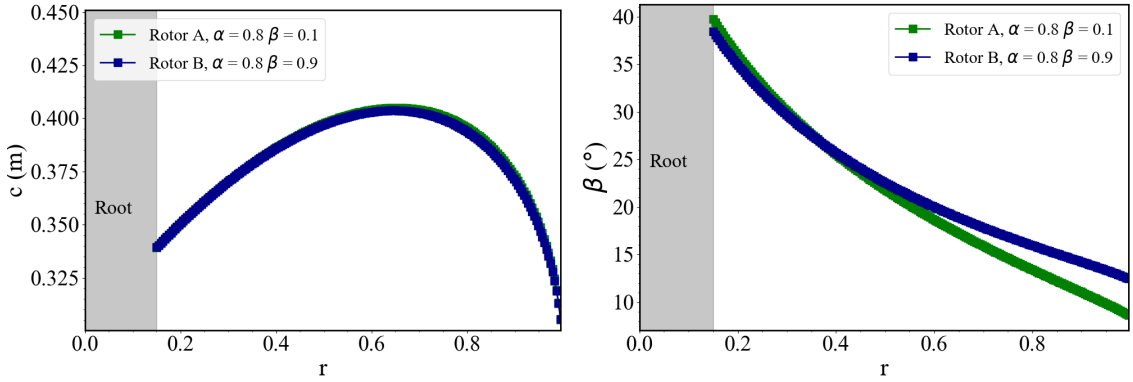


**(a) Chord distribution.** **(b) Twist distribution.**

Downloaded by MIT LIBRARIES on January 21, 2023 | http://arc.aiaa.org | DOI: 10.2514/6.2023-0209

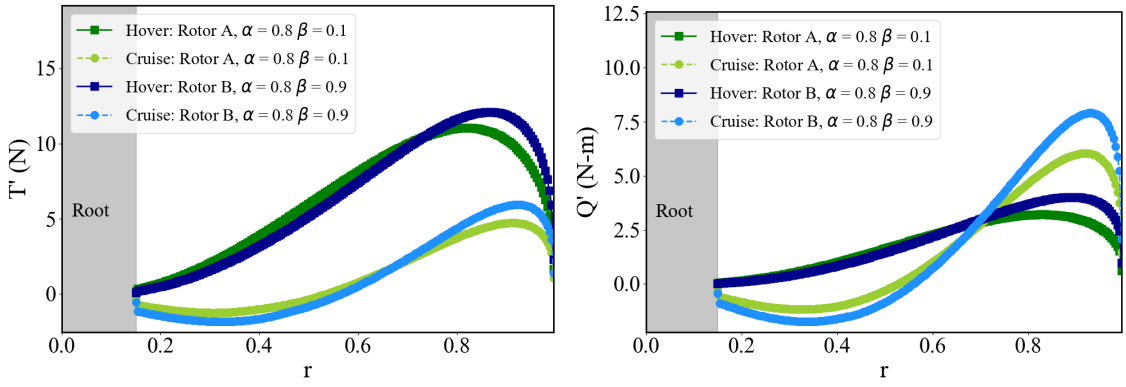


**(a) Thrust distribution.** **(b) Torque distribution.**

**Fig. 15 Prop-rotor planforms and performance at a constant $\alpha$ of 0.8.**

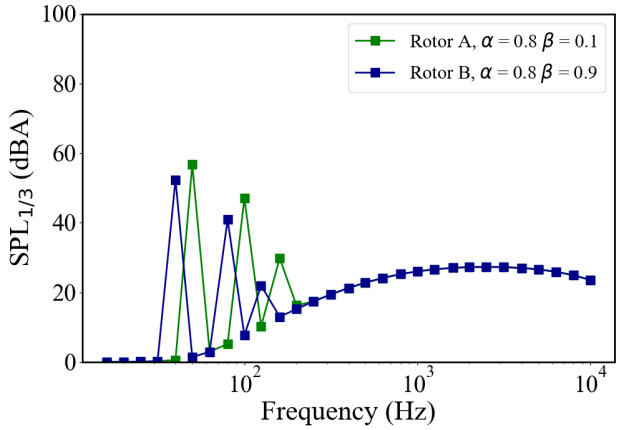


**Fig. 16 ⅓ Octave band spectra of prop-rotors at a constant $\alpha$ of 0.8.**

## VII. Future Work

This study showed how Pareto optimal rotors can be designed considering aerodynamics and aeroacoustics. The simple discretization scheme provided smooth rotor shapes and the inclusion of JIT compilation and AD further accelerated the optimization process. However, there are still some physical trade-offs to consider.

In the optimization process, we assumed taper ratio constraints as a stand-in for a true structural constraint. Crucially, we need to ensure that the blades will not fail under normal and emergency use. Furthermore, the blade shapes have a significant effect on the weight of the blade. With ten or more rotors on eVTOL and slim weight margins, this should not be ignored totally. Therefore, structural weights should be a constraint and/or additional objective in the optimization process.

Rotor dynamics are not included in this formulation of the BEMT. Bending and torsion of the rotor can cause a deviation in results, especially under high loads such as OEI hover. These can be accounted for using simple beam methods to represent the blades. Furthermore, the blade dynamics of these rigid blades require strong hubs to counter the moments produced. When considering larger eVTOL concepts weight savings could be found by utilizing semi-rigid or hinged rotors typically found on helicopters.

The airfoils of the rotor are held fixed at a NACA 4412, but future optimization processes should be able to also optimize the airfoil shape. While SUAVE can and does calculate the airfoil properties including boundary layer properties for aeroacoustics, these properties are pre-calculated for the optimization process. Coupled rotor/airfoil design with SUAVE could enable CFD levels of design results in mere minutes.

The acoustics properties presented here are only of an isolated rotor. This does capture the first-order noise effects. However, eVTOL configurations are much more complex. Determining the interactions of rotors to rotors and rotor to



Downloaded by MIT LIBRARIES on January 21, 2023 | http://arc.aiaa.org | DOI: 10.2514/6.2023-0209

airframe could affect on the overall design.

Finally, the promising results of utilizing JAX with SUAVE in optimization further motivate the developers to continue expanding its role within SUAVE. Future work includes coupled rotor/wing aerodynamic and acoustic optimization, airfoil optimization, trajectory optimization, and full vehicle and mission optimization concurrently. Bringing the optimization time down, while crucially maintaining high levels of fidelity is the end goal of this work.

## VIII. Conclusion

In this work we presented multi-objective optimization of rotors considering both aerodynamics and aeroacoustic considerations in the context of eVTOL design. We utilize a new elliptical based parameterization and incorporating Automatic Differentiation with just-in-time compilation via JAX. The combination of this reformulation and new code structure in SUAVE showed a clear advantage to both robustness and computational time. This faster optimization time and robust convergence enable designers to very quickly perform conceptual design studies on rotor blades at a medium level of fidelity.

We demonstrate the ability to design rotors for as either both pure lift rotors as well as propeller-rotors that combine cruise considerations. In these studies we illustrate how vastly different of a result is provided depending on the weighting of objectives including between aerodynamics and aeroacoustics as well as hover verse cruise performance. With these results and methods we empower the designer to quantify and better choose their optimal tradeoff in performance for their vehicle design. We hope with tools like these, that the emerging eVTOL industry can be kind to their neighbors.

Downloaded by MIT LIBRARIES on January 21, 2023 | http://arc.aiaa.org | DOI: 10.2514/6.2023-0209

## References


[1] Stivala, B., "'we're prisoners to this noise': Residents claim drone deliveries are driving them mad," , Sep 2022. URL https://9now.nine.com.au/a-current-affair/queensland-resident-fed-up-with-drone-delivery-noise/d2b32612-40ac-4fbf-a5c6-3a6c823b2c2d.

[2] Morgado, J., Abdollahzadeh, M., Silvestre, M., and Páscoa, J., "High altitude propeller design and analysis," *Aerospace Science and Technology*, Vol. 45, 2015, pp. 398–407.

[3] Stajuda, M., Karczewski, M., Obidowski, D., and Jóźwik, K., "Development of a CFD model for propeller simulation," *Mechanics and Mechanical Engineering*, Vol. 20, No. 4, 2016, pp. 579–593.

[4] Yamamoto, O., and August, R., "Structural and aerodynamic analysis of a large-scale advanced propeller blade," *Journal of Propulsion and power*, Vol. 8, No. 2, 1992, pp. 367–373.

[5] Caprace, D.-G., Cardoza, A., Ning, A., Mangano, M., He, S., and Martins, J. R., "Incorporating High-Fidelity Aerostructural Analyses in Wind Turbine Rotor Optimization," 2022, p. 1290.

[6] Betz, A., *Screw propellers with minimum energy loss*, NRC, Division of Mechanical Engineering, 1958.

[7] Goldstein, S., "On the vortex theory of screw propellers," *Proceedings of the Royal Society of London. Series A, Containing Papers of a Mathematical and Physical Character*, Vol. 123, No. 792, 1929, pp. 440–465.

[8] Glauert, H., "Airplane propellers," *Aerodynamic theory*, Springer, 1935, pp. 169–360.

[9] Theodorsen, T., "Theory of propellers," *Skipsmodelltankens meddelelse nr. 33, April 1954*, 1954.

[10] Larrabee, E. E., "Practical design of minimum induced loss propellers," *SAE Transactions*, 1979, pp. 2053–2062.

[11] Adkins, C. N., and Liebeck, R. H., "Design of optimum propellers," *Journal of Propulsion and Power*, Vol. 10, No. 5, 1994, pp. 676–682. doi:10.2514/3.23779, URL http://arc.aiaa.orghttp://arc.aiaa.org/doi/10.2514/3.23779.

[12] Ning, A., "Using blade element momentum methods with gradient-based design optimization," *Structural and Multidisciplinary Optimization*, Vol. 64, No. 2, 2021, pp. 991–1014.

[13] Ingraham, D., Gray, J. S., and Lopes, L. V., "Gradient-based propeller optimization with acoustic constraints," *Aiaa scitech 2019 forum*, 2019, p. 1219.

[14] Gur, O., and Rosen, A., "Optimization of propeller based propulsion system," *Journal of Aircraft*, Vol. 46, No. 1, 2009, pp. 95–106.

[15] Stoll, A., *Design of quiet UAV propellers*, Stanford University, 2012.

[16] Hanson, D. B., "Helicoidal surface theory for harmonic noise of propellers in the far field," *AIAA Journal*, Vol. 18, No. 10, 1980, pp. 1213–1220. doi:10.2514/3.50873.

[17] Lui, J., and McVeigh, M., "Design of swept blade rotors for high-speed tiltrotor application," *Aircraft Design and Operations Meeting*, 1991, p. 3147.

[18] Traub, L. W., Botero, E., Waghela, R., Callahan, R., and Watson, A., "Effect of taper ratio at low Reynolds number," *Journal of Aircraft*, Vol. 52, No. 3, 2015, pp. 734–747. doi:10.2514/1.C032559.

[19] Drela, M., "QPROP Formulation," 2006. URL `https://web.mit.edu/drela/Public/web/qprop/qprop_theory.pdf`.

[20] Erhard, R., Clarke, M., and Alonso, J., "A low-cost aero-propulsive analysis of distributed electric propulsion aircraft," *AIAA Scitech 2021 Forum*, Vol. 1 PartF, 2021.

[21] Clarke, M. A., Erhard, R. M., and Alonso, J. J., "Aerodynamic Optimization of Wing-Mounted Propeller Configurations for Distributed Electric Propulsion Architectures," 2021, pp. 1–19. doi:10.2514/6.2021-2471.

[22] Spera, D. A., "Models of lift and drag coefficients of stalled and unstalled airfoils in wind turbines and wind tunnels," Tech. rep., Washington, D.C, 2008.

[23] Hanson, D., "Sound from a propeller at angle of attack: a new theoretical viewpoint," *Proceedings of the Royal Society of London. Series A: Mathematical and Physical Sciences*, Vol. 449, No. 1936, 1995, pp. 315–328.

[24] Clarke, M., "Towards a Regional and Urban Air Mobility Future: The Development of Computational Approaches for Quantifying Trade-offs in Electric Aircraft Design," , 2022.

[25] Amiet, R. K., "Noise due to turbulent flow past a trailing edge," *Journal of Sound and Vibration*, Vol. 47, No. 3, 1976, pp. 387–393. doi:10.1016/0022-460X(76)90948-2.

[26] (Kevin) Li, S., and Lee, S., "Prediction of Urban Air Mobility Multirotor VTOL Broadband Noise Using UCD-QuietFly," *Journal of the American Helicopter Society*, Vol. 66, No. 3, 2021, pp. 1–13. doi:10.4050/jahs.66.032004.

[27] Lee, S., "Empirical wall-pressure spectral modeling for zero and adverse pressure gradient flows," *AIAA Journal*, Vol. 56, No. 5, 2018, pp. 1818–1829. doi:10.2514/1.J056528.

[28] Lukaczyk, T. W., Wendorff, A. D., Colonno, M., Economon, T. D., Alonso, J. J., Orra, T. H., and Ilario, C., "SUAVE: an open-source environment for multi-fidelity conceptual vehicle design," *16th AIAA/ISSMO Multidisciplinary Analysis and Optimization Conference*, 2015, p. 3087.

[29] Botero, E. M., Wendorff, A., MacDonald, T., Variyar, A., Vegh, J. M., Lukaczyk, T. W., Alonso, J. J., Orra, T. H., and Ilario da Silva, C., "Suave: An open-source environment for conceptual vehicle design and optimization," *54th AIAA aerospace sciences meeting*, 2016, p. 1275.

[30] Vegh, J. M., Botero, E., Clark, M., Smart, J., and Alonso, J. J., "Current capabilities and challenges of NDARC and SUAVE for eVTOL aircraft design and analysis," *2019 AIAA/IEEE Electric Aircraft Technologies Symposium (EATS)*, IEEE, 2019, pp. 1–19.

[31] Botero, E. M., and Alonso, J. J., "Conceptual Design and Optimization of Small Transitioning UAVs using SUAVE," *18th AIAA/ISSMO Multidisciplinary Analysis and Optimization Conference*, 2017, p. 4149.

[32] Bradbury, J., Frostig, R., Hawkins, P., Johnson, M. J., Leary, C., Maclaurin, D., Necula, G., Paszke, A., VanderPlas, J., Wanderman-Milne, S., and Zhang, Q., "JAX: composable transformations of Python+NumPy programs," , 2018. URL `http://github.com/google/jax`.

[33] Smart, J. T., and Alonso, J. J., "CPU Parallelization and GPU Acceleration of SUAVE: Advancements in Sampling and Optimization," *AIAA Scitech 2021 Forum*, 2021, p. 1356.

[34] Wu, N., Kenway, G., Mader, C. A., Jasa, J., and Martins, J. R. R. A., "pyOptSparse: A Python framework for large-scale constrained nonlinear optimization of sparse systems," *Journal of Open Source Software*, Vol. 5, No. 54, 2020, p. 2564. doi:10.21105/joss.02564.

[35] Gill, P. E., Murray, W., and Saunders, M. A., "SNOPT: An SQP algorithm for large-scale constrained optimization," *SIAM review*, Vol. 47, No. 1, 2005, pp. 99–131.

[36] Yu, P.-L., "Cone convexity, cone extreme points, and nondominated solutions in decision problems with multiobjectives," *Journal of Optimization Theory and Applications*, Vol. 14, No. 3, 1974, pp. 319–377.

[37] Kochenderfer, M. J., and Wheeler, T. A., *Algorithms for optimization*, Mit Press, 2019.

Downloaded by MIT LIBRARIES on January 21, 2023 | http://arc.aiaa.org | DOI: 10.2514/6.2023-0209